Investigation of microwave transitions and nonlinear magneto-optical rotation in anti-relaxation-coated cells*

D. Budker,[1,2,†] L. Hollberg,[3] D. F. Kimball,[1] J. Kitching,[3,‡] S. Pustelny,[4] H. G. Robinson,[3] and V. V. Yashchuk[5]

[1]*Department of Physics, University of California at Berkeley, Berkeley, California 94720-7300*
[2]*Nuclear Science Division, Lawrence Berkeley National Laboratory, Berkeley, California 94720*
[3]*National Institute of Standards and Technology, 325 S. Broadway, Boulder, CO 80305-3322*
[4]*Instytut Fizyki im. M. Smoluchowskiego, Uniwersytet Jagielloński, Reymonta 4, 30-059 Krakow, Poland*
[5]*Advanced Light Source Division, Lawrence Berkeley National Laboratory, Berkeley CA 94720*

(Dated: June 14, 2004)

Using laser optical pumping, widths and frequency shifts are determined for microwave transitions between the components of the ground-state hyperfine structure for ^{85}Rb and ^{87}Rb atoms contained in vapor cells with alkane anti-relaxation coatings. The results are compared with data on Zeeman relaxation obtained in nonlinear magneto-optical rotation (NMOR) experiments, a comparison important for quantitative understanding of spin-relaxation mechanisms in coated cells. By comparing cells manufactured over a forty-year period we demonstrate the long-term stability of coated cells, which may be useful for atomic clocks and magnetometers.

PACS numbers: 32.30.Bv,32.70.Jz,32.80.Bx,95.55.Sh

I. INTRODUCTION

Alkali metal vapor cells with paraffin anti-relaxation coatings, first introduced by H. G. Robinson et al. in the 1950's [1] and subsequently studied in great detail by M.-A. Bouchiat et. al. [2, 3] and other authors (see, for example, Ref. [4] and references therein), are presently at the heart of some of the most sensitive optical-pumping magnetometers [5]. Recently, paraffin-coated cells have also been used in investigations of nonlinear-optical effects such as nonlinear magneto- and electro-optical effects (see Refs. [6, 7] for detailed reviews). Although the use of paraffin-coated cells in atomic clocks has also been extensively investigated (see, for example, Refs. [8–10]), up until now such cells have not been commonly used in commercial clocks. Wall-coated cells have microwave clock-resonance linewidths comparable to those observed in cells containing buffer gases resulting in comparable short-term instability for cm-scale frequency references. In addition, the sensitivity of the resonance frequency to temperature variations is comparable for the two methods of confining the optically-pumped atoms (with the gas composition in the case of buffer-gas cells chosen to minimize the temperature dependence). However, wall coated cells are somewhat less robust than buffer-gas cells in that they must be kept at a temperature below that at which the wax melts. In addition, solid or liquid alkali metal which migrates onto the walls of the cell after it has been made can reduce the effectiveness of the wall coating, so care should be exercised to keep the coating temperature above or equal to that of the stem containing the condensed alkali metal. Thus it appears that for cm-scale frequency references, wall coatings have no distinct advantage over buffer gases in confining the atoms and there are certain drawbacks associated with cell reliability.

The ongoing work aimed at developing highly miniaturized atomic frequency references [11, 12] and magnetometers has created renewed interest in wall coatings. These devices will likely take advantage of miniature atomic vapor cells with physical dimensions on the order of 1 mm or smaller [13]. Because of the larger surface-to-volume ratio, atoms confined in such a small cell spend a larger fraction of their time interacting with the cell wall than they would in a larger cell. Therefore, linewidth broadening and frequency shifts associated with the cell walls can significantly affect the performance of the frequency reference even when a buffer gas of moderate pressure is used. Therefore, the quality and efficiency of coatings applied to the walls of such small cells is an important factor in determining the feasibility of highly miniaturized frequency references, particularly those with cell volumes significantly below 1 mm^3.

Collisions of alkali atoms with cell walls can affect the atomic state in a number of ways. In addition to optical resonance broadening, the atomic ground states can undergo spin (Zeeman) depolarization, hyperfine population transfer and hyperfine decoherence. Typically, the hyperfine decoherence rate (which includes hyperfine population transfer) is found to be about one order of magnitude larger than the Zeeman decoherence rate [9, 14]. It has also been observed that the hyperfine population transfer rate is significantly smaller than the overall hyperfine decoherence rate [15]. For atomic frequency references, the properties of the atomic transition between hyperfine levels determine the short-term stability, while for most magnetometers, transitions between Zeeman levels within a single hyperfine level are important. As a result, a comparison between different

†Electronic address: budker@socrates.berkeley.edu
‡Electronic address: kitching@boulder.nist.gov

wall-relaxation effects, particularly a comparison of Zeeman and hyperfine decoherence, is of interest both from the viewpoint of understanding the basic physics and also with regard to practical applications.

In this paper, we present measurements of intrinsic linewidths and shifts with several alkane-coated alkali-vapor cells manufactured in different laboratories over a period of about 40 years. We compare the results to those of the nonlinear magneto-optical rotation (NMOR [6]) experiments, and draw conclusions pertaining to the clock applications of the coated cells. Specifically, we find that wall coatings can remain effective for at least several decades after the cell is fabricated, and that the method by which the wall coating is applied has little bearing on the effectiveness of the coating (as long as the coating is of sufficiently high quality). In addition, the NMOR linewidth is found to be a factor of up to ten smaller than the hyperfine coherence linewidth when the two are measured in the same cell (at similar temperatures). This can be explained by the way in which electron-spin randomization contributes to the decoherence in each of these cases.

II. MICROWAVE-TRANSITION MEASUREMENTS

A schematic of the apparatus is shown in Fig.1. We used a distributed-Bragg-reflector (DBR) diode laser [16] with the measured linewidth of $\approx$ 2 MHz, whose frequency was tuned near the Rb D1 resonance (795 nm). After passing through a variable attenuator and an optical isolator used to avoid optical feedback into the laser, the light beam goes through a linear polarizer. It is then directed through a vapor cell (at room temperature) enclosed in a single-layer cylindrical magnetic shield. The laser beam diameter at the location of the cell is $\sim$ 7 mm. The intensity of the transmitted light is detected with a photodiode. A dc magnetic field is applied to the cell in the direction collinear with light propagation by passing current through a coil wound on the surface of a cylindrical acrylic insert (not shown) fitting into the magnetic shield. A microwave field is applied with a single-wire loop terminating a coaxial cable. The microwave synthesizer is referenced to a hydrogen maser ($\delta\nu/\nu \sim 10^{-13}$).

For one cell (TT11 [38], see Table I), a slightly different apparatus was used. The magnetic shield consisted of two layers, and a low-Q (of several thousand) cylindrical microwave cavity operating in the TE_{011} mode was employed instead of the wire loop. In addition, in this arrangement, it was possible to heat the cell while keeping the stem at a lower temperature. This was useful for evaluating the effect of the temperature on the widths and shifts of the microwave transition.

In the experiment, in the presence of a dc magnetic field, the laser frequency was tuned to a particular location on the optical absorption profile, and the microwave frequency was swept around the nominal frequency of the field-free separation of the ground-state hyperfine components of ^{85}Rb: 3,035,732,440 Hz [17] or ^{87}Rb: 6,834,682,610.9 Hz [18], while the transmitted light intensity was recorded. Examples of the experimental microwave spectra are shown in Figs. 2 and 3.

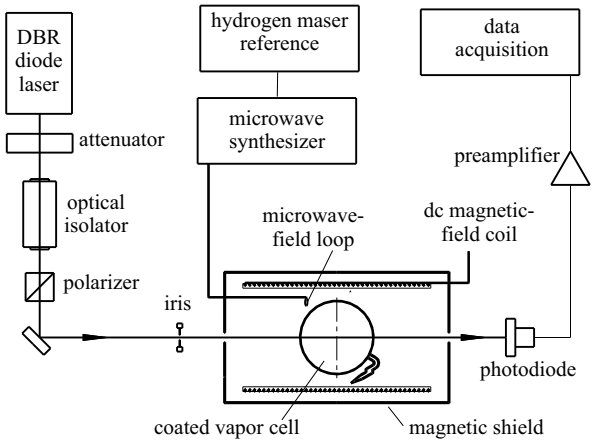

FIG. 1: Experimental setup for measuring microwave transitions.

The anti-relaxation-coated buffer-gas-free cells used in the present work are listed in Table I. None of these cells were "re-cured" or heat treated before testing (a procedure that may be used, if necessary, to control possible alkali metal that had collected on the coated walls).

The cell identified in Table I as Gib, containing a natural mixture of Rb isotopes, was manufactured at Berkeley around 1964 for the Ph.D. thesis work of H. M. Gibbs [19] (Ref. [19] gives a detailed description of the cell manufacturing process). The material is Paraflint which consists of alkane chains with a wide range of molecular weights. The coating was applied by melting Paraflint wax and running it over the cell surface. This cell has obvious Rb crystalline deposits on the wall and there are several glass tubulations on the spherical surface (i.e., imperfections that originate from glass tubes that were attached to the cell during the manufacturing process). Regions of the cell have heavy pooling of wax and the coating thickness is very non-uniform.

The cell referred to as Ale-10 cell was made by E. B. Alexandrov and M. V. Balabas according to the procedure described, for example, in Ref. [20]. The material of the coating is a mixture of alkane chains of different length fractionated from polyethylene at 220°C. The coating was applied by deposition from the vapor. The resulting coating has estimated thickness of $\sim$ 10 μm, and can be barely seen by eye.

The cells referred to as TT11 and H2 were made by H. G. Robinson. The material of the coating is tetracontane distilled at about 200°C. The purified tetracontane wax was evaporatively coated onto the cell surface from a hot needle. The resulting coating is thin (so it is not visible by eye) ; with melting temperature of $\sim$ 80°C.

TABLE I: Vapor cells used for the measurements and the experimentally determined values for microwave linewidths and shifts. T - the temperature of the cell (which was higher than that for the stem for some of the measurements). n - the total number density of Rb vapor. The quantity ϕ is the estimated average phase shift per wall collision. The uncertainty in ϕ includes an estimate of the effect of non-ideal cell shape. For ^{87}Rb, the phase shift ϕ' scaled to ^{85}Rb (see text) is also given. The last two columns list the deduced contributions to the microwave linewidths from the spin-exchange collisions and the adiabatic collisions, respectively (see text).

Cell	Year made	Ref.	Diam. (cm)	T (°C)	n (cm^{-3})	Isotope	$\frac{\gamma^{\mu}_{exp}}{2\pi}$ (Hz)	Shift (Hz)	$\lvert\phi\rvert$ (rad)	$\lvert\phi'\rvert$ (rad)	$\frac{\gamma^{\mu}_{se}}{2\pi}$ (Hz)	$\frac{\gamma^{\mu}_{a}}{2\pi}$ (Hz)
Ale-10	1997	[20]	10	25	$8\cdot10^9$	^{85}Rb	8.7(5)	-24(4)	0.037(7)		1.3	2
Gib	1964	[19]	10	25	$8\cdot10^9$	^{85}Rb	11(2)	-14(4)	0.022(6)		1.3	0.6
						^{87}Rb	16(4)	-42(2)	0.065(6)	0.029(3)	1.2	5
H2	1985	[21]	3.5	21	$7\cdot10^9$	^{87}Rb	22(3)	-93(1)	0.050(5)	0.022(2)	1.2	9
TT11	1985	[21]	3.4	22	$6.5\cdot10^9$	^{87}Rb	23(2)	-80(1)	0.043(4)	0.019(2)	1.0	7
				42	$1.4\cdot10^{10}$		17.5(10)				2.2	
				43	$3.4\cdot10^{10}$		21.5(10)	-70.5(3)	0.036(4)	0.016(2)	5.2	5

TABLE II: Experimentally determined values for FM NMOR linewidths. T - the temperature of the cell (the stem and the cell body are at the same temperature). n - the total number density of Rb vapor. γ^{NMOR}_{se} - calculated spin-exchange contribution to the NMOR linewidth. The last column lists the deduced contributions to the microwave linewidths from electron-spin-randomization collisions (see text).

Cell	T (°C)	n (cm^{-3})	Isotope	$\gamma^{NMOR}_{exp}/(2\pi)$ (Hz)	$\gamma^{NMOR}_{se}/(2\pi)$ (Hz)	$\gamma^{\mu}_{er}/(2\pi)$ (Hz)
Ale-10	19	$4\cdot10^9$	^{85}Rb	0.7(1)	0.15	3
	25	$6\cdot10^9$		1.2(1)	0.24	5
Gib	21	$4\cdot10^9$	^{85}Rb	2.9(1)	0.15	13
			^{87}Rb	2.9(1)	0.24	9
H2	21	$4\cdot10^9$	^{87}Rb	3.5(1)	0.24	11

III. NONLINEAR MAGNETO-OPTICAL MEASUREMENTS OF ZEEMAN RELAXATION

For several cells where we studied microwave transitions, we also measured Zeeman relaxation rates using nonlinear magneto-optical rotation. The general idea of the method (see the review [6] for a detailed discussion) is the following. The interaction of the atoms with a near-resonant laser field results in polarization of the atomic medium. The induced polarization evolves in the presence of a magnetic field and the resulting change of the medium's polarization is detected by measuring optical rotation of the light (which, in this case, plays the functions of both the pump and the probe). In this work, we use a version of the NMOR technique where the frequency of the laser is modulated and optical rotation varying at the modulation frequency is detected (FM NMOR [22–24]; Fig. 4). A static magnetic field is applied along the light propagation direction; the light is linearly polarized. As a function of the modulation frequency, narrow resonances (Fig. 5) with widths dependent on the ground-state Zeeman relaxation rate appear in the synchronously detected optical-rotation signal when the modulation frequency is equal to twice the Larmor frequency (the factor of two is related to the two-fold spatial symmetry of the induced atomic alignment).

An advantage of the FM NMOR technique for measuring the Zeeman relaxation rate is that when a bias field is applied (as in the present case), the resonance curves are, to first order, insensitive to small transverse magnetic fields; eliminating a possible systematic-error source.

IV. PROCEDURE, RESULTS AND DISCUSSION

The total electronic angular momentum in the ground electronic state of rubidium is $J = 1/2$. For ^{85}Rb, the nuclear spin is $I = 5/2$. In a low dc magnetic field where nonlinear Zeeman shifts resulting from decoupling of hyperfine structure can be neglected, one generally expects to see 11 distinct resonance hyperfine transition frequencies between various linear-Zeeman-split sublevels of the upper and lower ground state hyperfine levels. (For ^{87}Rb, an atom with $I = 3/2$, there are 7 transition frequencies.) This is observed experimentally (the upper plot in Fig. 2). The relative intensities of various components depend the parameters (power, polarization, tuning) of the pump light, on the geometry and orientation of the microwave loop, and on the microwave power. Under typical conditions in this experiment, the peaks of the resonances correspond to an increase in absorption by several percent (the optical depth on resonance of the room-temperature cells is of order unity).

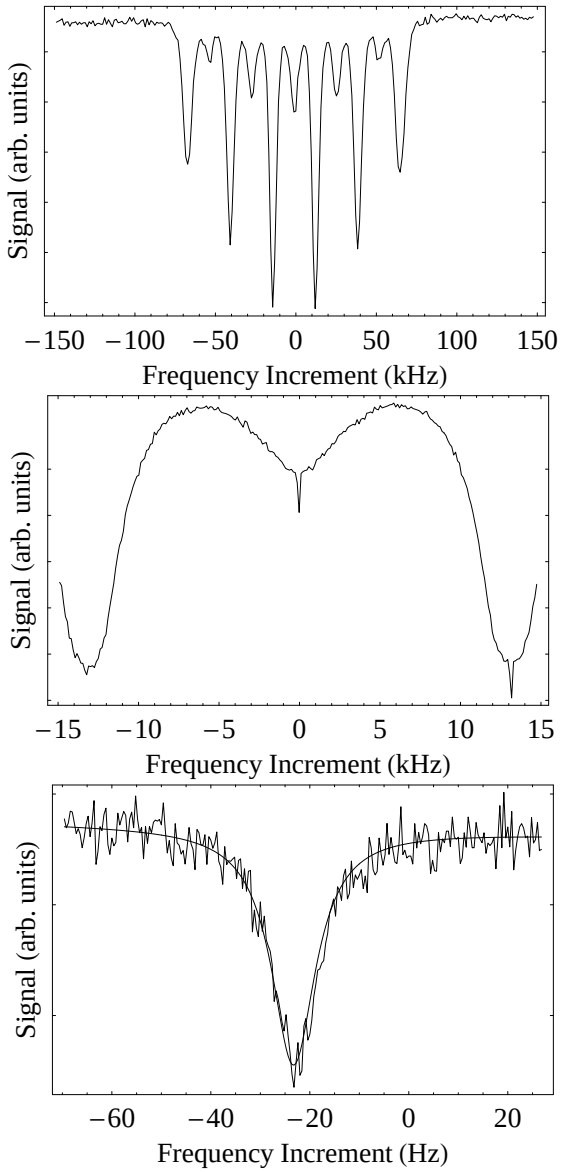

FIG. 2: Examples of the microwave spectra recorded with the Ale-10 ^{85}Rb cell (see Table I). The common parameters for the three scans are: dc magnetic field: 29 mG; linear light polarization, laser tuned to the center of the $F = 3 \rightarrow F'$ transition; total scan rate (saw-tooth sweep): 0.02 Hz. Each plot represents an average of approximately five scans. Upper and middle plots: input light power 0.25 μW; lower plot: input light power 13 μW, microwave power reduced by a factor ≈ 63. The lower plot also shows a fit with a Lorentzian superimposed on a linear background. The fit Lorentzian linewidth (FWHM) is 10.9(3) Hz, slightly larger than the "intrinsic" width of about 8.7 Hz (Table I) due to residual light broadening (see text).

The width of the peaks on the upper plot in Fig. 2 is about 4 kHz (FWHM) and is dominated by the Doppler width of the microwave transition and also contains a significant contribution due to the phase variation of the microwave field over the cell volume resulting from the use of a simple microwave loop. A zoom with higher frequency resolution (the middle plot in Fig. 2) reveals additional sharp features superimposed on top of the Doppler-broadened lines. These are the Dicke-narrowed lines [9, 25] of primary interest in the present work.

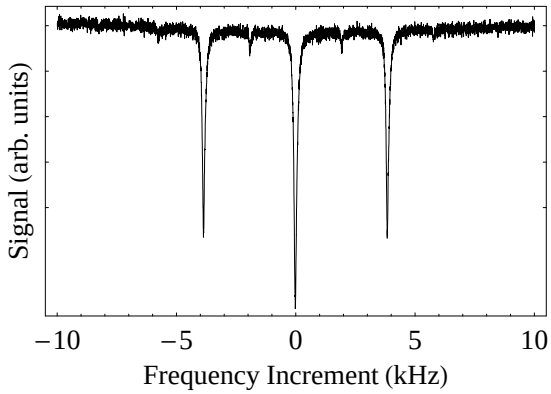

FIG. 3: An example of a microwave spectrum recorded with the TT11 ^{87}Rb cell (see Table I). The parameters for the scan are: dc magnetic field: 2.7 mG; linear light polarization, laser tuned to the center of the $F = 2 \rightarrow F'$ transition; total scan rate (saw-tooth sweep): 0.2 Hz. The plot represents a single scan. Input light power: 6 μW. The comparison of this plot with the middle plot in Fig. 2 illustrates the advantages of using a TE_{011} microwave cavity as opposed to a current loop: almost complete suppression of the broad pedestal and the $\Delta M_F \neq 0$ microwave transitions.

While all the sharp features are of comparable widths, in the following we concentrate on the central resonance corresponding to the "clock transition" between the $M = 0$ Zeeman components (the 0-0 transition), which is to first order insensitive to dc magnetic fields and gradients.

An example of a high-resolution recording of the narrow feature is shown in the lower plot in Fig. 2. The line shape is well described by a Lorentzian as seen from the fitting curve also shown in the plot.

We have investigated the widths and shifts of the central narrow resonance as a function of laser frequency tuning, laser polarization, and laser and microwave power. In particular, in order to eliminate the effects of power broadening and shifts, we performed double extrapolation of the widths and central frequencies of the resonances towards zero optical and microwave power. (In the limit of low light and microwave powers, we observe the expected linear dependences of the widths and shifts of the resonances on these powers, except for microwave-power shifts that are too small to be observed at the present sensitivity. The results for the "intrinsic" widths and shifts of the microwave transition (in the limit of zero light and microwave power and independent of laser tuning and polarization) are summarized in Table I. In the case of ^{85}Rb, uncertainties in the shifts include both the errors of the present measurement and 3 Hz uncertainty in the knowledge of the absolute tran-

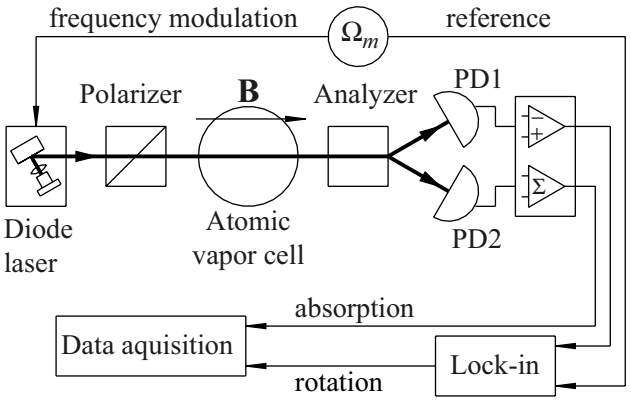

FIG. 4: Simplified schematic of the experimental setup for measuring Zeeman relaxation rate with the FM NMOR technique [22–24]. The vapor cell under study is placed inside a multi-layer magnetic shielding system (not shown) equipped with coils for compensating residual magnetic fields and gradients and for applying well-controlled fields to the cell. The time-dependent optical rotation is detected with a balanced polarimeter after the vapor cell. In this work, the laser was tuned to the Rb D1 line; laser beam diameter was ~ 2 mm, and the light power was $\lesssim 15$ μW.

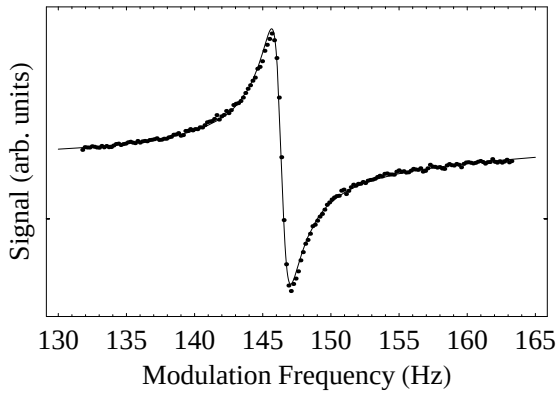

FIG. 5: An example of the FM NMOR data taken with the Ale-10 cell. The central frequency of the laser is tuned ≈ 400 MHz towards lower frequencies from the center of the $F = 3 \rightarrow F'$ absorption peak of the D1 line (this point corresponds to a maximum of the FM NMOR signal). The laser frequency is modulated with an amplitude of 20 MHz. A bias magnetic field of 156 μG is applied along the light-propagation direction. The data is shown along with a fit to a dispersive Lorentzian (see Ref. [24]). The width of the resonance corresponds to $\gamma_{exp}^{NMOR} = 2\pi \cdot 0.7$ Hz, the narrowest magneto-optical resonance width observed with alkali atoms to date.

sition frequency for free atoms [26]; for ^{87}Rb, the latter uncertainty is negligible [18].

As an experimental remark, we have found that, for example, for ^{85}Rb, tuning the laser frequency to the high-frequency slope of the $F = 3 \rightarrow F'$ optical transition allows one to greatly reduce light broadening, while retaining relatively large signals (the signal deteriorates on the low-frequency slope, presumably because Zeeman optical pumping dominates over hyperfine pumping). Similar "tricks" are also used in optical pumping magnetometry [27] and in NMOR [28, 29].

An example of the data taken with the microwave cavity is shown in Fig. 3. Using the TE_{011} cavity (as opposed to a microwave loop) has important advantages, as can be seen from the comparison of Fig. 3 with the middle plot in Fig. 2. In particular, strong suppression of the broad pedestal and the $\Delta M_F \neq 0$ microwave transitions is apparent. (In Ref. [10], microwave transition lineshapes were compared in the case of TE_{011} and TE_{111} cavities. It was found that narrow lines only appear in the former case. Ref. [10] also contains references to calculations of the lineshape in the regime where the dimensions of the cell are comparable with the wavelength, and, correspondingly, with the microwave cavity mode size.)

As an additional cross-check of the results given in Table I, a set of room temperature data for the H2 cell was also taken using the D2 resonance (780 nm; a different diode laser system was used for this measurement). The results, the intrinsic width of 20.3(9) Hz and shift of $-89.5(11)$ Hz are consistent with the data obtained with D1 resonance (see Table I), as expected.

The data taken at different temperatures in the TT11 cell provide some insight into the adsorption process of the alkali atoms on the walls. The adsorption time of the atom on the wall, under simplifying assumptions such as a uniform adsorption energy on all sites on the surface, is usually assumed to be [30]

$$\bar{t}_a = \tau_0 e^{E_a/kT}, \tag{1}$$

where τ_0 is the period of vibration of the adsorbed atom in the wall potential, E_a is the adsorption energy, k is the Boltzmann constant and T is the absolute temperature. At higher temperatures, therefore, an atom spends less time on the wall and should experience a smaller frequency shift and broadening. The frequency shift (discussed in the following section) in particular should be reduced by a factor equal to the fractional change in adsorption time due to the change in cell temperature:

$$\frac{d\Delta\nu}{\Delta\nu} = -\frac{E_a}{kT} \cdot \frac{dT}{T}. \tag{2}$$

For the TT11 cell, the frequency shift measured at two temperatures allows one to calculate [under the assumptions of Eq. (1)] the absorption energy, giving $E_a = 0.06$ eV. This is consistent with previous values found in similar cells but smaller than the 0.1 eV reported by some researchers (see Ref. [31] and references therein).

In interpreting the observed microwave frequency shifts we have assumed that these shifts originate in collisions of rubidium atoms with the cell walls because the cells studied here are nominally free from buffer gas. However, due to high mobility of helium atoms in glass, it is possible that atmospheric helium has diffused into the cells through the glass (particularly in the case of the

oldest Gib cell). If we assume that helium inside the cells is in equilibrium with the atmosphere where the partial He concentration is $5.2 \cdot 10^{-6}$, using the literature data for the frequency shifts of the rubidium 0-0 microwave transitions (e.g., Ref. [15]), we find that the microwave resonance is shifted by +1.3 Hz and +2.9 Hz for ^{85}Rb and ^{87}Rb, respectively. Since these shifts are relatively small, and since we do not know the actual pressure of helium in the cells, we ignore these shifts in the rest of the paper, noting them as a possible source of a small systematic error. Broadening due to collisions with helium is negligibly small.

The procedure for obtaining the Zeeman relaxation data is described in Refs. [22, 24]. Great care was exercised to minimize the possible contributions to resonance linewidths due to magnetic-field gradients. The contribution of gradient broadening to the FM NMOR linewidth (upon compensation of the gradients) is found to be negligible at the level of present uncertainties [32]. As in the case of microwave transitions, the observed resonance widths (see Fig. 5) were extrapolated to zero light power.

Atomic number densities listed in Tables I and II were determined by fitting absorption spectra taken at low light power.

V. INTERPRETATION

There are several known relaxation mechanisms present in these experiments, including spin-exchange relaxation, relaxation due to a finite probability of atoms going into the cell's stem containing uncoated surfaces, and wall collisions.

The contribution of the spin-exchange relaxation to the microwave width can be estimated using the formulae given in Refs. [33, 34]. For example, when only one isotope with nuclear spin I is present in the cell, the spin-exchange contribution to the linewidth of the 0-0 microwave transition is given by

$$\frac{\gamma^{\mu}_{se}}{2\pi} = \frac{R(I) n \overline{v}_{rel} \sigma_{se}}{\pi}, \tag{3}$$

where σ_{se} is the spin-exchange-collision cross-section ($\sigma_{se} = 2 \cdot 10^{-14}$ cm^2 for all cases relevant here [34]), n is the atomic number density,

$$\overline{v}_{rel} = \sqrt{8kT/\pi\mu_{red}} \tag{4}$$

is the average relative speed and μ_{red} is the reduced mass of the colliding atoms, and

$$R(I) = \frac{6I+1}{8I+4} \tag{5}$$

is the nuclear slow-down factor for the $0 \rightarrow 0$ transition. The values of the contribution of the spin-exchange collisions to the microwave linewidths deduced from the measured number density are listed in the last but one column of Table I. In all cases, this contribution is less than 25% of the overall observed linewidth γ^{μ}_{exp}.

The relaxation due to the stem can be estimated from the geometry (except for the Gib cell which does not have a stem, and where rubidium is apparently covered with paraffin), and is found to contribute to the microwave linewidth less than a fraction of a Hz in the case of the Ale-10 cell and less than one Hz in the case of the TT11 and H1 cells. Effects related to the cell stems therefore contribute to the hyperfine decoherence at a level somewhat less than the measurement errors given in Table I. We ignore this contribution in the following discussion.

Collisions of alkali atoms with the wall coating can be separated into three categories. The most "gentle" or adiabatic collisions, while causing hyperfine transition frequency shift and decoherence (as discussed below), generally are not accompanied by population transfer or Zeeman decoherence. The stronger collisions, for example, those with some paramagnetic impurities or "dangling bonds," randomize the electron spin. However, they do not affect the nuclear spin, so a polarized atom retains a certain degree of polarization after the collision. Finally, an atom can be absorbed into the coating for a sufficiently long time that all polarization is destroyed. Next we analyze the contribution of the adiabatic collisions.

While the adiabatic collisions do not cause atoms to jump between quantum states, the interaction with the wall during a collision causes a phase shift between hyperfine states, ϕ [30]. The hyperfine transition frequency shift due to this phase shift can be estimated as follows.

Consider an atom in the cell that we will track for a time τ much longer than the typical time interval between its wall collisions. The distance travelled by the atom (along some complicated reticulated trajectory) is $\overline{v}\tau$, where

$$\overline{v} = \sqrt{8kT/\pi M} \tag{6}$$

is the mean speed and M is the mass of the atom. The next question is: how many times did this atom collide with the wall? The answer for a spherical cell (for which the mean distance between wall collisions assuming the usual cosine angular distribution of atoms bouncing off the wall is $4R/3$) is

$$\frac{\overline{v}\tau}{4R/3} = \frac{\tau}{t_c}, \tag{7}$$

where t_c is the characteristic time between wall collisions. If the phase shift per collision is ϕ, the overall phase increment in time τ is:

$$\phi \frac{\overline{v}\tau}{4R/3}. \tag{8}$$

On the other hand, the phase increment is also equal to

$$2\pi\Delta\nu\tau, \tag{9}$$

TABLE III: Linewidth budget for the microwave transitions. $\gamma_a^\mu/(2\pi)$ and $\gamma_{er}^\mu/(2\pi)$ are the deduced contributions to the microwave linewidth from adiabatic and electron-randomization collisions (from Tables I and II), respectively. The last two columns list the total expected width based on the sum of these deduced contributions and the experimentally observed microwave linewidths (from Table I).

Cell	Isotope	$\gamma_a^\mu/(2\pi)$ (Hz)	$\gamma_{er}^\mu/(2\pi)$ (Hz)	Total (Hz)	$\gamma_{exp}^\mu/(2\pi)$ (Hz)
Ale-10	^{85}Rb	2	5	7	8.7(5)
Gib	^{85}Rb	0.6	13	14	11(2)
	^{87}Rb	5	9	14	16(4)
H2	^{87}Rb	9	11	20	22(3)

where $\Delta\nu$ is the sought for frequency shift. Equating (8) and (9), and cancelling τ, we get:

$$\Delta\nu = \frac{\phi}{2\pi}\frac{3\overline{v}}{4R}. \tag{10}$$

The values of the phase shift ϕ for various cells, experimental conditions, and Rb isotopes deduced from the experimental values of the microwave transition frequency shifts using Eq. (10) are listed in Table I. The results are consistent with the available earlier data for Rb in alkane-coated cells (Ref. [9] and references therein) within the spread between different cells under similar conditions and with the same Rb isotope.

In order to compare the coating properties for cells containing different isotopes (particularly, the Ale-10 cell with the other cells used in this work), one can scale the phase shift to one and the same isotope (e.g., ^{85}Rb) using the expected proportionality of the phase shift and the hyperfine transition frequency [39]. The scaled values (ϕ') for the ^{87}Rb data are listed in Table I. The results indicate that all the different coatings studied in this work produce roughly the same phase shifts in wall collisions. We also note that the phase shifts per collision measured here in Rb are roughly consistent with those measured for Cs on paraffin coatings ($\phi = 0.09(1)$ rad [30]), when scaled to the corresponding hyperfine frequency.

Because of the statistical character of the collisions, there is a spread in the amount of phase shift acquired by the atoms, which contributes to the resonance width [30, 35] (a derivation of the broadening and shift due to this mechanism is given in the Appendix):

$$\frac{\gamma_a^\mu}{2\pi} = \frac{\phi^2}{\pi t_c}. \tag{11}$$

For the parameters of the present experiment, these contributions to the width comprise from $\gamma_a^\mu/(2\pi) \approx 0.6$ Hz to ~ 10 Hz. As seen from Table I, the sums of γ_a^μ and γ_{se}^μ are insufficient to explain the observed overall intrinsic widths γ_{exp}^μ in any of the cases.

A possible contribution to the linewidth that may explain this "linewidth budget deficit" is from electron-spin randomizing collisions with the wall or, possibly, gaseous impurities (other than helium) [2]. The magnitude of this contribution to the width of the microwave transitions can be estimated from the NMOR linewidth. The measured NMOR linewidths are broader than what is expected given the known spin-exchange cross-sections (see Table II). It has been suggested that the dominant contribution to the width comes from spin-randomization collisions [36]. For the 0-0 microwave transition, in the case of electron randomization collisions, the relaxation rate of the 0-0 coherence should be 3/4 of the electron randomization rate [34], while the intrinsic NMOR linewidth due to electron-spin randomization is smaller due to the nuclear slow-down effect (see, for example, Ref. [34]) and is calculated to be $\approx 1/3$ of the spin-randomization rate for ^{85}Rb and $\approx 1/2$ for ^{87}Rb [36].

Using this information, the contribution of the electron-spin randomization collisions to the microwave linewidth can be estimated (γ_{er}^μ, Table II). For example, for the Ale-10 cell at 25°C, assuming that the Zeeman relaxation is dominated by spin-randomization collisions, we have

$$\frac{\gamma_{er}^\mu}{2\pi} \approx 2 \times (1.2 \text{ Hz}) \times 3 \times \frac{3}{4} \approx 5 \text{ Hz}. \tag{12}$$

(In the conditions of our experiments where linearly polarized low-intensity light is used, the effect of spin-exchange collisions is nearly identical to that of electron-randomization collisions [34], and we do not separate spin exchange from the additional electron-randomization processes in this estimate and those presented in Tables II and III.) In expression (12), the factor of two accounts for the relation between the relaxation rate for the 0-0 coherence and the Lorentzian width of the microwave transition. Adding up all the contributions and estimating the associated uncertainties, we find that for the Ale-10 cell we can account for about 7(1) Hz out of the observed 8.7(5) Hz, which is satisfactory, particularly, in view of a number of simplifying assumptions in our model (for example, the assumption that the dispersion of ϕ is equal to ϕ^2 in the adiabatic collisions, see Appendix, etc.). The microwave linewidth budgets for the cells where both the microwave and NMOR data are available are summarized in Table III.

The fact that both Rb isotopes are simultaneously present in the Gib cell allows one to check our model for consistency, and provides further evidence that the dispersion of phase shifts in adiabatic collisions is not the dominant source of the microwave linewidth. For the values of ϕ (Table I) for the two isotopes extracted from the

measured frequency shifts using Eq. (10), Eq. (11), predicts about an order of magnitude larger contribution to the width for ^{87}Rb, clearly inconsistent with a relatively small change of the width observed experimentally and the assumption that the phase shift dispersion dominates the width.

In conclusion of this Section, we note that assuming that the additional relaxation comes from the collisions that completely depolarize atoms rather than electron-randomization collisions, one does not achieve a satisfactory agreement between the microwave and NMOR linewidths.

VI. CONCLUSION

It appears that coatings manufactured by three rather different technologies studied in this work all show comparable performance in terms of the parameters (linewidth and shift) relevant to magnetometers and atomic clocks utilizing anti-relaxation-coated cell walls. Moreover, the fact that a cell (Gib) manufactured 40 years ago shows comparable performance to that of more recently manufactured cells is evidence of the stability of the coating properties [40] and suitability of such cells for extremely long term measurements, for example, as frequency reference and magnetic sensor elements for deep-space missions.

The durability of the wall coatings and the lack of dependence of the coating properties on the method of coating deposition are encouraging with regard to the application of such coatings to miniature atomic frequency references. It is clear that wall coatings might play an important role in improving the performance of compact atomic clocks if a way of integrating the application of the coating with the cell fabrication process is found. This integration will likely be an important future step in the development of atomic clocks based on sub-mm alkali atom vapor cells.

The present experimental data for the widths and shifts of the microwave transitions appears inconsistent with a hypothesis that the linewidth is dominated by dispersion of the phase shifts in adiabatic wall collisions. On the other hand, comparing the microwave data and the Zeeman relaxation data measured with nonlinear magneto-optical rotation, we have proposed that the dominant source of the linewidth is electron-spin randomizing collisions. This hypothesis consistently accounts for the linewidth-budget deficits for both microwave transitions and NMOR resonances. The rate of the electron-randomization collisions necessary to explain the observed microwave and NMOR linewidths are too large to be accounted for by spin-exchange collisions (Tables I and II). Thus, it is necessary to assume electron randomization processes occurring either in collisions of the alkali atoms with cell walls or, possibly, in collisions with gaseous impurities. These two scenarios may be distinguished by comparing relaxation rates for otherwise similar cells having vastly different diameters. This will be addressed in future work.

The authors are grateful to D. English, S. M. Rochester, and J. E. Stalnaker for useful discussions and help with data analysis, to S. N. Evans for his help in understanding the statistics underlying collisional broadening and shift, and to H. Shugart, E. B. Alexandrov, and M. V. Balabas for providing the anti-relaxation-coated cells. This work was supported by the Office of Naval Research, NSF, by a CalSpace Minigrant, and by the Microsystems Technology Office of the Defence Advanced Research Projects Agency (DARPA). D.B. also acknowledges the support of the Miller Institute for Basic Research in Science.

VII. APPENDIX

Here we give a derivation of line broadening and shift arising due to the collisional phase shifts acquired by atoms.

Suppose atomic oscillators are all in phase initially, and in the absence of collisions, they all oscillate at a frequency ω_0. Let ϕ be the average phase shift per collision, and $1/t_c$ – the average collision rate. The phase shifts acquired by different atoms after a time $t \gg t_c$ are generally not the same because there are two factors that lead to a dispersion in this quantity. First, there is a statistical distribution of the number of collisions n experienced by atoms over a time t which we will assume Poissonian:

$$p(n,t) = \frac{e^{-t/t_c}(t/t_c)^n}{n!}, \tag{13}$$

where $p(n,t)$ is the probability that an atom experiences n collisions in time t [the mean number of collisions corresponding to the distribution (13) is $\langle n\rangle = t/t_c$]. Second, the phase shifts per collision are not the same. We will assume a normal distribution with a mean value ϕ ($|\phi| \ll 1$) and a dispersion ϕ^2. (The latter property follows from a distribution of wall-sticking times with a universal binding energy exceeding kT; see, for example, Ref. [30].)

Let us consider atoms that have experienced some fixed number of collisions $n \gg 1$. Let ϕ_n be the overall phase accumulated by an atom over n collisions. Because of the normal distribution of phase shifts in individual collisions (resulting in a random walk in phase), we have a Gaussian distribution of accumulated phases:

$$p(\phi_n, n) = \frac{1}{\sqrt{2\pi n\phi^2}} e^{-\frac{(\phi_n - n\phi)^2}{2n\phi^2}}, \tag{14}$$

where $n\phi$ is the average phase accumulated in n collisions, and $n\phi^2$ is the dispersion.

Taking into account the distributions (13) and (14), the oscillation amplitude averaged over the atomic ensemble is found as a weighted sum of the contributions from

individual atoms ($\propto e^{i(\omega_0 t+\phi_j)}$, where ϕ_j is the phase accumulated by this individual atom):

$$A(t) \propto \sum_{n=0}^{\infty} \frac{e^{-t/t_c}(t/t_c)^n}{n!} \int_{-\infty}^{\infty} \frac{e^{i(\omega_0 t+\phi_n)}}{\sqrt{2\pi n\phi^2}} e^{-\frac{(\phi_n - n\phi)^2}{2n\phi^2}} d\phi_n \quad (15)$$

$$= e^{i\omega_0 t - t/t_c\left(1-e^{-i\phi-\phi^2/2}\right)}, \quad (16)$$

where in the last step we have explicitly evaluated the integral and the sum. Next, we use the fact that $|\phi| \ll 1$, and, expanding the exponential factor to second order in ϕ, we obtain:

$$A(t) \propto e^{i(\omega_0 - \phi/t_c)t - \phi^2 t/t_c}, \quad (17)$$

which says that the frequency of the oscillation is shifted by ϕ/t_c, and the amplitude decays at a rate ϕ^2/t_c leading to line broadening [41]. In order to obtain the line width of the absorption resonance, the decay rate of the amplitude has to be multiplied by a factor of two. Therefore, Eq. (17) proves the formulae (10) and (11).

[1] H. Robinson, E. Ensberg, and H. Dehmelt, Bull. Am. Phys. Soc. **3**, 9 (1958).

[2] M. A. Bouchiat, Ph.D. thesis, L'Universite de Paris (1964).

[3] M. A. Bouchiat and J. Brossel, Phys. Rev. **147**(1), 41 (1966).

[4] V. Liberman and R. J. Knize, Phys. Rev. A **34**(6), 5115 (1986).

[5] E. B. Alexandrov and V. A. Bonch-Bruevich, Opt. Eng. **31**(4), 711 (1992).

[6] D. Budker, W. Gawlik, D. F. Kimball, S. M. Rochester, V. V. Yashchuk, and A. Weis, Rev. Mod. Phys. **74**(4), 1153 (2002).

[7] E. B. Aleksandrov, M. Auzinsh, D. Budker, D. F. Kimball, S. M. Rochester, and V. V. Yashchuk, *Dynamic effects in nonlinear magneto-optics of atoms and molecules* (2004), physics/0405049.

[8] A. Risley, J. Jarvis, S., and J. Vanier, J. Appl. Phys. (USA) **51**(9), 4571 (1980).

[9] H. G. Robinson and C. E. Johnson, Appl. Phys. Lett. **40**(9), 771 (1982).

[10] R. P. Frueholz, C. H. Volk, and J. C. Camparo, J. Appl. Phys. (USA) **54**(10), 5613 (1983).

[11] J. Kitching, S. Knappe, and L. Hollberg, Appl. Phys. Lett. **81**, 553 (2002).

[12] Y. Y. Jau, A. B. Post, N. N. Kuzma, A. M. Braun, M. V. Romalis, and W. Happer, Phys. Rev. Lett. **92**(11), 110801/1 (2004).

[13] L. Liew, S. Knappe, J. Moreland, H. G. Robinson, L. Hollberg, and J. Kitching, Appl. Phys. Lett. **84**(14), 2694 (2004).

[14] H. G. Robinson and C. E. Johnson, IEEE Trans. Instrum. Meas. **IM-32**, 198 (1983).

[15] J. Vanier, J. F. Simard, and J. S. Boulanger, Phys. Rev. A **9**(3), 1031 (1974).

[16] T. Hirata, M. Maeda, M. Suehiro, and H. Hosomatsu, IEEE J. Quantum Electron. **27**(6), 1609 (1991).

[17] M. Tetu, R. Fortin, and J. Y. Savard, IEEE Trans. Instrum. Meas. **25**, 477 (1976).

[18] S. Bize, Y. Sortais, M. S. Santos, C. Mandache, A. Clairon, and C. Salomon, Europhys. Lett. **45**(5), 558 (1999).

[19] H. M. Gibbs, Ph.D. thesis, University of California, Berkeley (1965).

[20] E. B. Alexandrov, M. V. Balabas, D. Budker, D. English, D. F. Kimball, C. H. Li, and V. V. Yashchuk, Phys. Rev. A **66**(4), 042903/1 (2002).

[21] H. G. Robinson (1985), unpublished.

[22] D. Budker, D. F. Kimball, V. V. Yashchuk, and M. Zolotorev, Phys. Rev. A **65**, 055403 (2002).

[23] V. V. Yashchuk, D. Budker, W. Gawlik, D. F. Kimball, Y. P. Malakyan, and S. M. Rochester, Phys. Rev. Lett. **90**, 253001 (2003).

[24] Y. P. Malakyan, S. M. Rochester, D. Budker, D. F. Kimball, and V. V. Yashchuk, Phys. Rev. A **69**(1), 013817 (2004).

[25] R. Dicke, Phys. Rev. **89**, 472 (1953).

[26] J. Vanier and C. Audoin, *The quantum physics of atomic frequency standards* (A. Hilger, Bristol ; Philadelphia, 1989).

[27] E. B. Aleksandrov, M. V. Balabas, and V. A. Bonch-Bruevich, Pis'ma Zh. Tekh. Fiz. **13**(11-12), 749 (1987).

[28] D. Budker, V. Yashchuk, and M. Zolotorev, Phys. Rev. Lett. **81**(26), 5788 (1998).

[29] D. Budker, D. F. Kimball, S. M. Rochester, V. V. Yashchuk, and M. Zolotorev, Phys. Rev. A **62**(4), 043403 (2000).

[30] H. M. Goldenberg, D. Kleppner, and N. F. Ramsey, Phys. Rev. **123**(2), 530 (1961).

[31] C. Rahman and H. G. Robinson, IEEE J. Quantum Electron. **QE-23**(4), 452 (1987).

[32] S. Pustelny, D. F. Kimball, V. V. Yashchuk, and D. Budker (2004), to be published.

[33] F. Grossetete, J. Phys. (Paris) **29**(5-6), 456 (1968).

[34] W. Happer, Rev. Mod. Phys. **44**(2), 169 (1972).

[35] R. Jochemsen, M. Morrow, A. J. Berlinsky, and W. N. Hardy, Phys. Rev. Lett. **47**(12), 852 (1981).

[36] A. I. Okunevich, S. M. Rochester, D. Budker, and V. V. Yashchuk (2003), unpublished. Indirect evidence that electron-spin-randomization collisions are significant comes also from an experimental comparison of relaxation rates for the quadrupole and hexadecapole moments for the case of ^{87}Rb in a paraffin-coated cell similar to the Ale-10 cell, see V.V. Yashchuk, D. Budker, W. Gawlik, D.F. Kimball, Yu. P. Malakyan, and S.M. Rochester, Phys. Rev. Lett. **90**, 253001 (2003).

[37] R. Herman and H. Margenau, Phys. Rev. **122**, 1204 (1961).

[38] This cell was kindly loaned to us by Symmetricom, TRC. This does not imply an endorsement by NIST; cells from other companies may work equally well.

[39] This neglects possible effects of the different mass of the two isotopes. The proportionality of the phase shift and the hyperfine frequency arises from the fact that the mechanism through which the phase shift occurs is the

change of the valence-electron density near the nucleus during a collision [30, 37]. This scaling is confirmed, at least approximately, by the present work (see the data for the two Rb isotopes simultaneously present in the Gib cell listed in Table I), and the earlier work of Ref. [15].

[40] For example, assuming that the intrinsic coating properties at a certain time after manufacturing were identical for the Ale-10 and the Gib cell, we can roughly estimate the temporal drift of the microwave frequency shift as being ≤ 10 Hz/30 years.

[41] It is interesting to note that neglecting either one of the random factors – the number of collisions experienced by an atom or the dispersion in phase shift per collision – leads to a two times slower decay rate in either case.